Entropy generation analysis of hybrid-nanofluid during natural convection through two coaxial cylinders partially filled with porous medium under magnetic field

Y . Foukhari [1,*] , M. Sammouda [1], M. Driouich [1]

[1] Research laboratory in physics and sciences for engineering, LRPSI

Sultan Moulay Slimane university, Polydisciplinary faculty, Beni Mellal, 23000, Morocco

[*] Corresponding author: Youness.foukharifpb@usms.ma

January 18, 2024

Abstract

The aim of this research is to analyze the magneohydrodynamic heat transmission in an annular space partially porous between two cencentric cylinders with a permeable interface saturated by a hybrid nanofluid (water-Cu/Al_2O_3) and study the entropy generation to better understand the heat transfer processes. The inner and outer cylinders are kept at a constant hot and cold temperature. The base walls are designed to be impermeable and insulated. A finite difference-based vorticity-stream function is used to solve the nonlinear coupled conservation equations using Successive Over Relaxation approach. The obtained numerical outcomes in terms of streamlines, isotherms, Nusselt and Bejan numbers, and entropy generation are presented to demonstrate the effect of various control parameters. The findings of this numerical simulation show that the enhance in the Ra number improves thermal energy transmission across the active wall. Further, a rise in nanoparticle concentration causes a rise in thermal conductivity, which contributes to enhancing the heat transfer rate. In addition, the mean entropy generation elements rise with increasing Rayleigh number, Darcy number, and nanoparticle concentration; however, with the exception of magnetic irreversibility, the reverse development is detected. Furthermore, the Bejan number is reduced in order to increase the Rayleigh and Darcy numbers.

Keywords: Natural convection, Entropy generation, Hybrid nanofluid , Magnetic field, Porous medium.

1 Introduction

Over the last few years, magnetohydrodynamic (MHD) heat transmission has remained an exciting issue for researchers because of its numerous applications in diverse areas such as geothermal energy, electronics, and many others. However, the researchers discovered a limitation in ordinary liquids, for example, oil, water, and ethylene glycol; which have a reputation for having poor heat conductivity. To develop thermal conductivity, they invented an innovative type of thermal transfer liquid called nanofluids by mixing nanoparticles in various base fluids. Choi [1] was the one who originally used the term ”nanofluids” for this novel category of fluids with excellent thermal properties. Eastman et al. [2] investigated the thermal conductivity improvement of (Cu-ethylene glycol) nanofluid. They noted that the addition of copper nanoparticles enhanced the thermal

Nomenclature

AL	Aspect ratio	ϕ	Nanoparticle concentration
R_i	Inner radius	$\phi 1$	Aluminium concentration
R_e	Outer radius	$\phi 2$	Copper concentration
H	Cavity height	Ω, ψ	Vorticity, Stream function
Cp	specific capacity	$\overline{\Omega}, \overline{\psi}$	Dimensionless vorticity, stream function
r,z	Dimensional coordinates	Σ, Λ	Nanofluid constant
$\overline{r}, \overline{z}$	Dimensionless coordinates	ΔT	Temperature difference
Xp	Porous layer thickness	T,$\overline{T}$	Temperature, Dimensionless temperature
Be	Bejan number	g	Gravity acceleration
λ	Thermal coductivity	Γ	Effective viscosity
σ	Electrical conductivity	**Subscripts**	
μ	Dynamic viscosity	hnf	Hybrid nanofluid
$\xi 1$	The irreversibility Coefficient	nf	Nanofluid
U,W	Dimensional velocity component	np1	Aluminium nanoparticle
$\overline{U}, \overline{W}$	Dimensionless velocity component	np2	Copper nanoparticle
Ha	Hartmann number	eff	Effective
k	Porous medium permeability	Loc	Local
Da	Darcy number	Avg	Average
B_0	Magnetic field	c	Cold
Pr	Prandtl number	h	Hot
Nu	Nusselt number	p	Porous medium
S_{gen}	Entropy generation	bf	Base fluid
Ra	Rayleigh number	ϵ	Porous medium
α	Thermal diffusivity	Th	Thermal
β	Thermal expansion coefficient	ff	Fluid friction
ρ	Density	Mag	Magnetic

conductivity. The movement of nanofluid through a lid-driven rectangle enclosure is supplied by Tiwari and Das [3] who investigated the manners of nanofluids by taking the nanoparticle concentration into account. Vajravelu et al. [4] demonstrated convective heat transfer in nanofluids of Cu-water and Ag-water, which the boundary layer thickness drops faster for Ag-water. Foukhari et al. [5] explored natural convection in an annular space between two coixial cylinders partially filled with a porous medium and submerged in a nanofluid Cu-water. Another investigation looks at the different ways in which the shape of the nanoparticles influences heat transfer [6,7]. Furthermore, a great deal of research has been undertaken on nanofluids, although hybrid nanofluids have not been addressed. It should be emphasized that their applications have attracted the interest of researchers in going beyond the limits of nanofluids. Numerous studies, both numerical and experimental, have looked at the use of a hybrid nanofluid in various situations for convective heat transfer [8–10]. Sheikholeslami et al. [11,12] proved that electrical output increases with loading MWCNT particles and also analyzed the possibility of utilizing a permeable zone for the discharging expedition.

Another potentially efficient method for reducing and managing the rate of heat transfer was represented by convective heat transfer related to magnetic force, which attracted the attention of researchers. The magnetic force combines with the buoyancy flux of an electrically conductive fluid to produce the Lorentz force, which influences heat transmission processes. Roy [13] investigated free convection flow and heat transfer in a rectangular container saturated by a hybrid nanofluid under numerous heating sources in the presence of a magnetic force. Mebarek-Oudinaa et al. [14,15] conducted a numerical study of magnetohydrodynamic natural convection in a vertical porous cylindrical cavity full of magnetic nanofluid. They arrived at the conclusion that increased magnetic force reduces heat transfer. Parvin et al. [16] discovered many forms of parameter effects in secondary flow, such as the Grashof number and the Prandtl number, when considering nanoparticles passing through the annulus. Furthermore, Selimefendigil et al. [17,18] examined the effects of combining the use of a magnetic field with rotating cylinders on the thermal processes and phase transitions in a T-shaped branching channel. In addition, several studies have evaluated how heat transfer in an magnetohydrodynamics (MHD) flow is affected by the suspension of nanoparticles and the impact of internal heat generation [19–22]. El Glili and Driouich [23] examined the effect of variable viscosity on the flow of electromagnetohydrodynamic Casson nanofluid, taking into account Brownian motion and the thermophoresis effect. Sheremet et al. [24] examined other numerical studies of free convection in an undulating porous region in the presence of a steady magnetic field.

Furthermore, a different strategy was discovered by combining various mediums, which were separated based on the application, either vertically or horizontally, which has attracted the interest of researchers and investigated the influences of interface conditions, stress jump, and stress continuity at the interface [25–29]. On the other hand, many studies are using the Darcy-Birnkman model to analyze the effect of porous media [30,31]. Foukhari et al. [32] attempted to comprehend the behavior of the nanofluid in a particular geometry by investigating the MHD natural convection between two vertical concentric cylinders. Chamkha et al. [33] expanded the problem by taking into account fully developed micropolar natural convection fluid flow in a vertical channel. In the biomedical application, Vijatha and Reddy [34] illustrated the construction of entropy generation, heat transport, and flow characteristics of blood flow in a Darcy-Forchheimer stretched cylinder. Karimi et al. [35] conducted an analytical investigation of forced convection in a space that was subjected to a uniform heat flux and partially submerged by a porous material. Mahmoudi et al. [36,37] evaluated the thermal behavior of a channel featuring a centrally located porous zone. Chamkha [38] investigated analytically the transient and hydromagnetic fluid flow processes for heat transfer properties in circular pipes and channels adopting a two-phase continuum approach. Other studies on non-Darcian fully developed flow and with variable porosity are improving our understanding of the impact of intricate flow phenomena on a wide range of porous media applications [39–41].

Entropy generation analysis, which acts as a criteria for assessing irreversibilities because of various sources and effects in a fluid domain, is another important topic for researchers. As a result, optimizing thermal engineering systems necessitates not only optimizing heat transfer performance but also optimizing entropy generation. Bejan [42] has worked hard to bridge the gap between thermodynamics, heat transfer, and fluid mechanics. He used the second law of thermodynamics to calculate the entropy creation caused by heat and flow transport in a cavity. Akhter et al. [43] embarked on an investigation of the entropy production of a magnetoconvective flow within a porous cavity filled with a hybrid nanofluid in the presence of an external magnetic field. Additional studies examine how the dynamic interaction of entropy generation and magnetohydrodynamics affects the thermal behavior and sense of evolution of systems in a variety of situations [44–51]. In a computational investigation, Ramasekhar and Reddy [52] examined the importance of electro-magnetohydrodynamic Darcy-Forchheimer hybrid nanofluid flow across a permeable rotating disk with radiation and heat generation.

This study investigates the impact of an externally oriented magnetic force on entropy generation and heat transmission. The primary goals are to express hybrid nanofluid flow by studying the annular space between two coaxial cylinders, predict entropy formation pace, and implement innovative uses of nanoparticles and controlled range to regulate fluid flow, heat transfer, and entropy generation. The aim is to meet the growing need for thermal effectiveness in the 4th industrial movement.

2 Mathematical approach

2.1 Mathematic formulation and boundary condition

Figure 1 represents a vertical coaxial cylinders with height H, with a saturated Newtonian hybrid nanofluid (water-Cu/Al_2O_3) partially filled with a porous layer with thickness Xp. The outside cylinder is kept at a constant cold temperature, while the inner cylinder is maintained at a uniform hot temperature. Furthermore, the solid and nanofluid are assumed to be in thermal equilibrium ($Tp = T_{hnf}$) [32]. The flow is intended to be a laminar, homogeneous, incompressible, and isotropic porous medium with uniform physical properties, except for density estimated using the Boussinesq approximation. The ion slip effect and Hall current are neglected. [53–55].

The current study's dimensional mathematical formulation is in vector form.

For the porous layer:

$$\triangledown.\overrightarrow{V} = 0, \tag{1}$$

$$\frac{1}{\epsilon^2}\overrightarrow{V}.\triangledown\overrightarrow{V} = -\frac{1}{\rho_{hnf}}\triangledown p - \frac{\mu_{hnf}}{\rho_{hnf}.K}\overrightarrow{V} + \frac{\mu_{hnf}}{\rho_{hnf}.\epsilon}\triangledown.\left(\triangledown.\overrightarrow{V}\right) - \beta_{Th}\left(T - Tc\right)\overrightarrow{g} - \frac{\sigma_{hnf}}{\rho_{hnf}}B_0^2\overrightarrow{V}, \tag{2}$$

$$\overrightarrow{V}.\triangledown T = \alpha_{eff}\triangledown.\left(\triangledown T\right). \tag{3}$$

For the nanofluid layer:

$$\triangledown.\overrightarrow{V} = 0, \tag{4}$$

$$\overrightarrow{V}.\triangledown\overrightarrow{V} = -\frac{1}{\rho_{hnf}}\triangledown p + \frac{\mu_{hnf}}{\rho_{hnf}}\triangledown.\left(\triangledown.\overrightarrow{V}\right) - \beta_{Th}\left(T - Tc\right)\overrightarrow{g} - \frac{\sigma_{hnf}}{\rho_{hnf}}B_0^2\overrightarrow{V}, \tag{5}$$

$$\overrightarrow{V}.\triangledown T = \alpha_{hnf}\triangledown.\left(\triangledown T\right). \tag{6}$$

By using the rotational operator $\overrightarrow{\Omega} = \overrightarrow{rot}\overrightarrow{V}$, the controlling equations in scalar form are derived from the expressions of the stream function and vorticity [56]. To normalize them, the following non-dimensional parameters are provided [57]. With m refers to hnf or eff.

$$\left(\overline{r};\overline{z}\right) = \left(\frac{r}{R_e};\frac{z}{R_e}\right) ; \left(\overline{U};\overline{W}\right) = \left(\frac{UR_e}{\alpha_m};\frac{WR_e}{\alpha_m}\right) ; \overline{\Omega} = \frac{\Omega.R_e^2}{\alpha_m} ; \overline{\Psi} = \frac{\Psi}{\alpha_m R_e} ; \overline{S} = \frac{T_0 R_e^2}{\lambda_{bf}\Delta T^2}$$
$$\overline{T} = \frac{(T - T_f)}{\Delta T = (T_c - T_f)} \tag{7}$$

For the porous layer:

$$\frac{1}{\overline{r}}\frac{\partial(\overline{rU})}{\partial\overline{r}} + \frac{\partial\overline{W}}{\partial\overline{z}} = 0, \tag{8}$$

$$\frac{1}{\epsilon^2}\left(\frac{\partial(\overline{U}\overline{\Omega})}{\partial\overline{r}}+\frac{\partial(\overline{W}\overline{\Omega})}{\partial\overline{z}}\right)=-\Lambda\overline{\lambda}^2 RaPr\frac{\partial\overline{T}}{\partial\overline{r}}+\left(-\overline{\lambda}.\Sigma\frac{Pr}{Da}-\overline{\lambda}.\Gamma.\Sigma\frac{Pr}{\overline{r}^2}\right)\overline{\Omega}$$
$$+\overline{\lambda}.\Gamma.\Sigma.Pr\left(\frac{\partial^2\overline{\Omega}}{\partial\overline{r}^2}+\frac{1}{\overline{r}}\frac{\partial\overline{\Omega}}{\partial\overline{r}}+\frac{\partial^2\overline{\Omega}}{\partial\overline{z}^2}\right) \tag{9}$$
$$-\overline{\lambda}.\frac{\sigma_{hnf}}{\sigma_{bf}}.Ha^2.Pr_{bf}\frac{\Sigma}{(1-\phi)^{-2.5}}\frac{\partial\overline{U}}{\partial\overline{z}},$$

$$\frac{\partial(\overline{U}\overline{T})}{\partial\overline{r}}+\frac{\partial(\overline{W}\overline{T})}{\partial\overline{z}}+\frac{\overline{U}\overline{T}}{\overline{r}}=\frac{\partial^2\overline{T}}{\partial\overline{r}^2}+\frac{1}{\overline{r}}\frac{\partial\overline{T}}{\partial\overline{r}}+\frac{\partial^2\overline{T}}{\partial\overline{z}^2}. \tag{10}$$

For the nanofluid layer:

$$\frac{1}{\overline{r}}\frac{\partial(\overline{r}\overline{U})}{\partial\overline{r}}+\frac{\partial\overline{W}}{\partial\overline{z}}=0, \tag{11}$$

$$\frac{\partial(\overline{U}\overline{\Omega})}{\partial\overline{r}}+\frac{\partial(\overline{W}\overline{\Omega})}{\partial\overline{z}}=\Sigma.Pr\left(\frac{\partial^2\overline{\Omega}}{\partial\overline{r}^2}+\frac{1}{\overline{r}}\frac{\partial\overline{\Omega}}{\partial\overline{r}}-\frac{\overline{\Omega}}{\overline{r}^2}+\frac{\partial^2\overline{\Omega}}{\partial\overline{z}^2}\right)-\Lambda.Ra.Pr.\frac{\partial\overline{T}}{\partial\overline{r}}$$
$$-\frac{\sigma_{hnf}}{\sigma_{bf}}.Ha^2.Pr_{bf}\frac{\Sigma}{(1-\phi)^{-2.5}}\frac{\partial\overline{U}}{\partial\overline{z}}, \tag{12}$$

$$\frac{\partial(\overline{U}\overline{T})}{\partial\overline{r}}+\frac{\partial(\overline{W}\overline{T})}{\partial\overline{z}}+\frac{\overline{U}\overline{T}}{\overline{r}}=\frac{\partial^2\overline{T}}{\partial\overline{r}^2}+\frac{1}{\overline{r}}\frac{\partial\overline{T}}{\partial\overline{r}}+\frac{\partial^2\overline{T}}{\partial\overline{z}^2}. \tag{13}$$

Where,

$$\Gamma=\frac{\mu_{eff}}{\mu_{hnf}},\quad \alpha_{hnf}=\frac{\lambda_{hnf}}{(\rho Cp)_{hnf}},\quad \alpha_{eff}=\frac{\lambda_{eff}}{(\rho Cp)_{eff}},\quad \overline{\lambda}=\frac{\lambda_{hnf}}{\lambda_{eff}},\quad \lambda_{eff}=(1-\epsilon)\lambda_p+\epsilon\lambda_{hnf}. \tag{14}$$

$$\Sigma=\frac{(1-\phi 1)^{-2.5}.(1-\phi 2)^{-2.5}.\left(\frac{(\rho C)_{hnf}}{(\rho C)_{bf}}\right)}{\frac{\lambda_{hnf}}{\lambda_{bf}}\left(\frac{\rho_{hnf}}{\rho_{bf}}\right)},\qquad \Lambda=\frac{\frac{(\rho\beta)_{hnf}}{(\rho\beta)_{bf}}}{\frac{\rho_{hnf}}{\rho_{bf}}.\left(\frac{\lambda_{hnf}}{\lambda_{bf}}.\frac{(\rho C)_{bf}}{(\rho C)_{hnf}}\right)^2}. \tag{15}$$

The dimensionless parameters in the preceding Equations 9 and 12 can be written as:

$$Ra=\frac{\rho_{bf}.g.\beta_{Th}.\Delta T.R_e^3}{\mu_{bf}\alpha_{bf}},\qquad Ha=R_eB_0\sqrt{\frac{\sigma_{bf}}{\mu_{bf}}},\qquad Pr=\frac{\mu_{bf}}{\rho_{bf}\alpha_{bf}},\qquad Da=\frac{k}{R_e^2}. \tag{16}$$

The boundary condition:

$$\begin{cases}\overline{T}=1,\quad \overline{\psi}=\frac{\partial\overline{\psi}}{\partial\overline{r}}=\frac{\partial\overline{\psi}}{\partial\overline{z}}=0,\quad \overline{\Omega}=\frac{2}{\Delta\overline{r}^2}\overline{\psi}|_{\Delta\overline{r}}. & At\,\overline{r}=R_i\,,\ 0\le\overline{z}\le H.\\ \overline{T}=0,\quad \overline{\psi}=\frac{\partial\overline{\psi}}{\partial\overline{r}}=\frac{\partial\overline{\psi}}{\partial\overline{z}}=0,\quad \overline{\Omega}=\frac{2}{\Delta\overline{r}^2}\overline{\psi}|_{0.5-\Delta\overline{r}}. & At\,\overline{r}=R_e\,,\ 0\le\overline{z}\le H.\\ \frac{\partial\overline{T}}{\partial\overline{z}}=0,\quad \overline{\psi}=\frac{\partial\overline{\psi}}{\partial\overline{r}}=\frac{\partial\overline{\psi}}{\partial\overline{z}}=0,\quad \overline{\Omega}=\frac{2}{\Delta\overline{r}^2}\overline{\psi}|_{\Delta\overline{z}}. & At\,R_i\le\overline{r}\le R_e\,,\ \overline{z}=0.\\ \frac{\partial\overline{T}}{\partial\overline{z}}=0,\quad \overline{\psi}=\frac{\partial\overline{\psi}}{\partial\overline{r}}=\frac{\partial\overline{\psi}}{\partial\overline{z}}=0,\quad \overline{\Omega}=\frac{2}{\Delta\overline{r}^2}\overline{\psi}|_{AL-\Delta\overline{z}}. & At\,R_i\le\overline{r}\le R_e\,,\ \overline{z}=H.\end{cases} \tag{17}$$

$$\begin{cases}\overline{T}_{hnf}=\overline{T}_p,\quad \frac{\partial\overline{T}_{hnf}}{\partial\overline{r}}=\frac{\lambda_{eff}}{\lambda_{hnf}}\frac{\partial\overline{T}_p}{\partial\overline{r}}.\\ \overline{\psi}_{nf}=\overline{\Psi}_p,\quad \frac{\partial\overline{\psi}_{nf}}{\partial\overline{r}}=\frac{\mu_{eff}}{\mu_{hnf}}\frac{\partial\overline{\psi}_p}{\partial\overline{r}}. & At\quad \overline{r}=R_i+X_p,\ 0\le\overline{z}\le H.\\ \overline{\Omega}_{hnf}=\overline{\Omega}_p,\quad \frac{\partial\overline{\Omega}_{nf}}{\partial\overline{r}}=\frac{\mu_{eff}}{\mu_{hnf}}\frac{\partial\overline{\Omega}_p}{\partial\overline{r}}.\end{cases} \tag{18}$$

The active wall's rate of heat transfer coefficient is expressed using the average Nusselt number [58], as provided by:

$$Nu_{Avg} = \frac{1}{AL}\frac{\lambda_{eff}}{\lambda_{bf}}\int_0^{AL}\frac{\partial \overline{T}_{hnf}}{\partial \overline{r}}d\overline{z}. \tag{19}$$

2.2 Thermophysical propreties

The study proposes a hybrid nanofluid model by mixing copper nanoparticles with alumina in water as a base fluid. Alumina nanoparticles are added to the core solution at a fixed concentration $\phi 1 = 0.01$. Table 1 shows the current and proposed valid thermophysical characteristics of the nanofluid and hybrid nanofluid [59].

2.3 Entropy generation

The irreversible nature of heat transport and viscosity factors cause the fluid to generate entropy continuously. The development of entropy is therefore due to the non-equilibrium flow forced by the cavity's boundary conditions. With the inclusion of an additional outside force (the magnetic force), the rate of entropy creation (which comes from energy and entropy balances) for a bidimentional flow is given in its general form as follows:

$$S_{gen} = \frac{k_{hnf}}{T_0^2}\left[\left(\frac{\partial T}{\partial r}\right)^2 + \left(\frac{\partial T}{\partial z}\right)^2\right] + \frac{\mu_{hnf}}{T_0}\left[2\left(\left(\frac{\partial U}{\partial r}\right)^2 + \left(\frac{\partial W}{\partial z}\right)^2\right) + \left(\frac{\partial U}{\partial z} + \frac{\partial W}{\partial r}\right)^2\right] + \frac{\sigma_{hnf}B_0^2U^2}{T_0}. \tag{20}$$

According to this process, and to be able to derive a dimensionless modeling of local entropy generation in free convection in the presence of a magnetic force, which will contain three components:

$$\overline{S}_{Loc} = \overline{S}_{gen-th} + \overline{S}_{gen-ff} + \overline{S}_{gen-Mag}. \tag{21}$$

$$\begin{aligned}\overline{S_{Loc}} = &\frac{k_{hnf}}{k_{bf}}\left[\left(\frac{\partial \overline{T}}{\partial \overline{r}}\right)^2 + \left(\frac{\partial \overline{T}}{\partial \overline{z}}\right)^2\right] + \delta.\xi_1\left[2\left(\left(\frac{\partial \overline{U}}{\partial \overline{r}}\right)^2 + \left(\frac{\partial \overline{W}}{\partial \overline{z}}\right)^2\right) + \left(\frac{\partial \overline{U}}{\partial \overline{z}} + \frac{\partial \overline{W}}{\partial \overline{r}}\right)^2\right] \\ &+ \frac{\sigma_{hnf}}{\sigma_{bf}}\xi_2\left(\frac{\alpha_{hnf}}{\alpha_{bf}}\right)^2\overline{U}^2.\end{aligned} \tag{22}$$

Where,

$$\delta = \frac{\mu_{hnf}}{\mu_{bf}}\left(\frac{\alpha_{hnf}}{\alpha_{bf}}\right)^2, \qquad \xi_1 = \frac{\mu_{bf}T_0}{k_{bf}}\left(\frac{\alpha_{bf}}{R_e.\Delta T}\right)^2, \qquad \xi_2 = \xi_1.Ha^2. \tag{23}$$

$$\overline{S}_{gen} = \int\int \overline{S}_{Loc}drdz. \tag{24}$$

The following expression is the definition of the local and global Bejan number, which are defined by:

$$Be_{Loc} = \frac{\overline{S}_{g-th}}{\overline{S}_{Loc}}, \qquad Be_{Avg} = \int\int Be_{Loc}drdz. \tag{25}$$

3 Numerical approach

3.1 Numerical procedure

The sets of dimensionless governing equations related to the border conditions are complex and nonlinear; therefore, in order to obtain the streamlines and temperature distribution, they must be numerically solved. The energy and vorticity equations are resolved using the central differences approach. Following the discretization procedure, the controlling algebraic formulas are resolved using the Alternation Direction Implicit (ADI) approach. The equation for the stream function has been solved using the Successive Over Relaxation (SOR) method [60]. The iteration process was carried out repeatedly until the condition was met for the best average change across all dependent variables. The numerical simulation's flow chart is shown in Figure 2.

$$\frac{\sum_i \sum_j \mid f_{i,j}^{n+1} - f_{i,j}^{n} \mid}{\sum_i \sum_j \mid f_{i,j}^{n} \mid} \leq 10^{-5}. \tag{26}$$

Where f refers to temperature (T) and vorticity (Ω).

3.2 The Grid sensitivity test and code validation

The study conducts a grid sensitivity analysis to find a grid-independent solution. The average Nusselt number is determined for various mesh systems in Table 2, showing that a mesh size of (71×141) is suitable for grid independence. The numerical program is validated by comparing results with previous studies by Krane and Jessee [61], Abu Nada et al. [62] Figure 3, and Sankar et al. [63] Figure 4.

4 Results and discussion

In this research, we investigated the entropy generation in a hybrid nanofluid between two coaxial cylinders for an aspect ratio of ($AL = H/Re = 2$) , which was studied under an external magnetic force. It is saturated by a porous medium, whose porosity is adjusted to $\epsilon = 0.7$, which correlates to glass $\lambda_p = 0.845 W/m.K$. The hybrid nanofluid is constructed from combining of Cu and Al_2O_3 nanoparticles in base fluid, as illustrated by their characteristics in Table 3. The simulation is performed for the physical parameters listed as Darcy number, Hartmann number, Rayleigh number, and nanoparticle concentration with ranges of $10^{-5} \leq Da \leq 10^{-1}$, $0 \leq Ha \leq 150$, $10^3 \leq Ra \leq 10^6$, and $0.01 \leq \phi \leq 0.05$ successively.

Figure 5 illustrates the effect of Rayleigh number Ra on the temperature and streamline contours under an external unifom magnetic force (Ha = 50). It is shown in Figure 5 at $Ra = 10^4$, that the entire enclosure is filled with one clockwise circular cell with a low maximum intensity flow. Furthermore, a lower Ra number causes a reduced buoyancy impact, and thus the conduction mode has grown to be important in heat transport. Then, at $Ra = 10^5$ and 10^6, the streamline cycles are amplified and stretched with optimum strength, causing the nanofluid to go away from the warm side toward the cold side. For the temperature distribution via isotherm contours, as the space study was heated from the inner cylinder, a high temperature zone formed there, and the temperature distribution moved vertically into the outside, which demonstrated the dominance of the conduction mode. Further, an augments in Rayleigh number to 10^6 leads the pattern of the isotherms to be restructured and become more curved, which means that the convection mode becomes dominant. The most notable discovery is that the highest number of compact isotherms measures the high temperature zone adjacent to the hot wall, indicating higher heat transmission from the source.

Figure 6 illustrates how the magnetic force affected the heat transfer rate for $Ra = 10^5$. As seen in Figure 6, at Ha = 0, there is no magnetic field, which means there is no effect on heat transfer rate, and the intensity's flow in this case is $|\psi| = 5.56$. At Ha = 150, the stremlines were more affected than in the previous situations, and the flow circulation strength was reduced to $|\psi| = 2.35$. Lorentz's force, which is formed as a consequence of the reaction of magnetic force and hybrid nanofluid buoyancy flow, has the ability to slow the flow velocity within the hybrid nanofluid zone. Further, it implies that Lorentz's force has no significant effect on the isotherms, whereas Ha ranges from 0 to 50, while it shows an important shift when a magnetic force's strength rises to Ha = 150, which causes the isotherms to change shape from horizontal to almost vertical.

Figure 7 depicts the streamlines and isotherms for different Darcy values at constant magnetic field strength Ha = 50. The Darcy number provides a substantial effect on velocity and rate of heat transfer through the hybrid nanofluid region, taking into account that it is linked directly to the permeability of porous media. As shown in Figure 7, at $Da = 10^{-5}$, smaller Da values indicated less porosity of the annular, which leads to a rise in the velocity in the free region. This is because decreasing porosity causes most of the fluid to escape to the free zone, while the remaining fluid in the porous region is impeded and mixed owing to the hydraulic resistance of impediments in the porous region. With an increase to $Da = 10^{-3}$ and 10^{-1}, the medium becomes more permeable, allowing more nanofluid to pass through the porous layer [32], which leads to an increase in the cell's strength and enhancement in heat transfer, as seen in Figure 7.

4.1 Effect some control parameters on average Nusselt number

Figure 8 depicts the heat transfer rate using the Nu_{Avg} curves in the fluid flow region as physical factors vary. Figure 8(a-c) shows that Nu_{avg} rises as the Rayleigh number grows. The rate of heat transmission is observed to be slow increasing at $Ra = 10^3$ to 10^4 and then quick growing at $Ra \geqslant 10^4$. To better comprehend the increasing of Nu_{Avg}, it was calculated using the data presented in Figure 8b for $Ha = 30$ and discovered that the average Nusselt number boosts by 8.30% when Ra shifts from 10^3 to 10^4, 96.52% from 10^4 to 10^5, and 285,53% from 10^5 to 10^6. This is because a higher Rayleigh number causes a strong buoyancy effect, resulting in an increase in the velocity through the cavity and thus leading to the transport of more heat energy via the hybrid nanofluid region. The interaction of magnetic force and buoyancy flow decreases flow velocity and generates more heat inside the fluid region, which declines as magnetic field strength increases, as shown in Figure 8b, which we found a full agreement with the research of Akhter et al. [43]. In addition, an improving trend can be seen in Figure 8a for increasing Darcy number, which results in an increase in permeability and flow velocity.

In Figure 8c, the improvement in nanoparticle concentration increases the thermal conductivity of the hybrid nanofluid and, therefore, the potential for energy transport. According to the numerical outcomes of Figure 8(a-c), the rate of Nu_{Avg} at $Ra = 10^6$ declines by 15.1% for the magnetic parameter shifts from Ha = 0 to 100, and accelerates by 100% and 9.72% respectively for the enhancement of Darcy number from $Da = 10^{-5}$ to 10^{-2} and the augmentation of hybrid nanoparticle concentration from $\phi = 1\%$ to 5%. Consequently, the growth of the Nu_{Avg} caused by Ra number is slowed by boosting the Hartmann number but accelerated by boosting Darcy number and nanoparticles concentration.

4.2 Effect of some control parameters on different component of entropy.

Figure 9 depicts the entropy generation caused by heat transmission, fluid friction, and magnetic impact for various Ra numbers under different control parameters. As shown in Figure 9(a-i), the increase in Ra number causes an increase in entropy generation components, whether caused by heat transfer, fluid friction, and magnetic effect. It is vital to notice that the growth of the entropy generation components is minimal for $Ra \leq 10^5$ and maximum for $Ra \geqslant 10^5$ for the reason that convection impact was found to be weak and powerful for smaller and greater Rayleigh values, respectively. In Figure 9(b,e,h), the irreversibility of entropy creation owing to fluid friction and heat transfer is observed to diminish with enhancing magnetic force strength. The effects of a magnetic field significantly decrease buoyancy impact and, thus, convection heat transfer rate; consequently, fluid friction entropy and heat transfer entropy are reduced. In addition, as the study treated by [43], we were able to show that the average entropy generation components increase with increasing cavity permeability, as seen in Figure 9(a,d,g), which makes our outcomes more convincing. These situations are anticipated with an increasing Darcy number, which means that the hybrid nanofluid will have an easier time moving from the porous region to the hybrid nanofluid region, leading to an acceleration of the flow velocity and heat transfer process. Figure 9(c,f,i) describe the entropy generation components that result from the injection of hybrid nanoparticles into the base fluid. In which the fluid friction entropy and heat transfer entropy improve with an improvement in the hybrid nanoparticle concentration, and that's related to the viscosity , which corresponds to an increase in flow resistance. Also, the presence of hybrid nanoparticles in a fluid boosts entropy generation relating to the magnetic impact, in which the magnetic characteristics of the nanoparticles may interact with the magnetic field that is applied, causing extra forces that may result in turbulent flow behavior.

4.3 Effect some control parameters on Bejan number

Figure 10 represents the outcomes of the Be number for different Ra numbers at various control parameters. The Bejan number reduces dramatically as the irreversibility components grow with Ra. Furthermore, the greatest values of the Bejan number that are superior to 0.5 are identified at the smallest Ra number, meaning that heat transfer irreversibility takes over entropy generation, while the values of the Bejan number that are inferior to 0.5 are noticed at the highest Ra number, indicating that fluid friction and magnetic irreversibility take over entropy generation. Additionally, there is a direct correlation that combines the Bejan number and the hybrid nanoparticle concentration. It basically comes down to the notion that a higher dynamic viscosity is produced when there are more hybrid nanoparticles dispersed in the base fluid, which enhances energy dissipation in the fluid domain.

5 Conclusion

This study numerically investigates entropy generation by magneoconvection heat transfer in a specific configuration closer to industrial geometries. The study uses a hybrid nanofluid composed of Al_2O_3 and Cu nanoparticles. The finite difference approach is used to model the controlled equations, and the FORTRAN numerical code is used to treat the problem, verifying it with published numerical and experimental results. The main conclusions drawn from the results are as follows:

* Increasing the Ra number from 10^4 to 10^6 results in an improvement in thermal energy transmission of 285.53 %. In addition, a reduction of 15.1% is observed at $Ra = 10^6$ when the Ha number is increased from 0 to 100 and is accelerated by 100% when the Da number is increased from 10^{-5} to 10^{-2}.
* The flow is considerably influenced by the rise in Rayleigh number. The intensity of the streamlines augments rapidly at high Ra but decreases as the magnetic field strength increases.
* An increase in Darcy number generates a rapid increase in fluid flow circulation, rate of heat transfer, and entropy generation components; however, there is a decrease in Bejan number Be for all Ra number. Furthermore, the streamlines vary progressively as the Darcy number Da grows.
* Heat transmission and entropy generation components improve as Ra rises, but both drop as Hartmann number increases, with the exception of magnetic entropy.
* Entropy generation is predominated by heat transfer irreversibility for the smaller Ra number, whereas fluid friction irreversibility for the upper values of Ra.

Statements and Declarations

The datasets generated during and/or analysed during the current study are available from the corresponding author on reasonable request. The authors declare that no funds.

References

[1] Choi, S.U.S. "Enhancing thermal conductivity of the uids with nanoparticles", ASME Fluids Eng. Div., **231**, pp. 99-105 (1995).

[2] Eastman, J.A., Choi, S.U.S., Li, S., et al. "Anomalously increased effective thermal conductivity of ethylene glycol-based nanofluids containing copper nanoparticles", Appl. Phys. Lett. **78** , pp. 718-720 (2001).

[3] Tiwari, R. K., and Das, M. K. "Heat transfer augmentation in a two-sided lid-driven differentially heated square cavity utilizing nanofluid", Int. J. Heat Mass Transf, **50**, pp. 2002-2018 (2007).

[4] Vajravelu, K., Prasad, K. V., Lee, J., et al. "Convective heat transfer in the flow of viscous Ag-water and Cu-water nanofluids over a stretching surface", Int. J. Therm. Sci, **50**, pp. 843-851 (2011).

[5] Foukhari, Y., Sammouda, M., Driouich, M., et al. " Heat transfer by natural convection in an annular space partially porous layered and saturated by a nanofluid", AIP Conf. Proc. **2761**(1) pp. 040021 (2023).

[6] Foukhari, Y., Sammouda, M., Driouich, M., et al. "Nanoparticles Shape Effect on Heat Transfer by Natural Convection of Nanofluid in a Vertical Porous Cylindrical Enclosure Subjected to a Heat Flux. pp. 437-445 (2021).

[7] Sammouda, M., Gueraoui, K., Driouich, M., et al. "The effect of Al_2O_3 nanoparticles sphericity on heat transfer by free convection in an annular metal-based porous space between vertical cylinders submitted to a discrete heat flux", J. Porous Media, **25**(2), (2022).

[8] Selimefendigil, F., and Chamkha, A. J. "Natural convection of a hybrid nanofluid-filled triangular annulus with an opening,Computational Thermal Sciences", An International Journal, **8**(6), (2016).

[9] Madhesh, D., and Kalaiselvam, S. "Experimental analysis of hybrid nanofluid as a coolant", Procedia Eng. **97**, pp. 1667-1675 (2014).

[10] Chamkha, A. J., and Al-Naser, H. "Double-diffusive convection in an inclined porous enclosure with opposing temperature and concentration gradients", Int. J. Therm. Sci., **40**(3), pp. 227-244 (2001).

[11] Sheikholeslami, M. "Numerical investigation for concentrated photovoltaic solar system in existence of paraffin equipped with MWCNT nanoparticles", Sustainable Cities and Society, **99**, pp. 104901 (2023).

[12] Sheikholeslami, M., and Khalili, Z. "Investigation of solar Photovoltaic cell utilizing hybrid nanofluid confined jet and helical fins for improving electrical efficiency in existence of thermoelectric module", Appl. Therm. Eng, **234**, pp. 121329 (2023).

[13] Roy, N. C. "MHD natural convection of a hybrid nanofluid in an enclosure with multiple heat sources", Alex. Eng. J, **61**(2), pp. 1679-1694 (2022).

[14] Mebarek-Oudina, F., and Bessaïh, R. "Oscillatory magnetohydrodynamic natural convection of liquid metal between vertical coaxial cylinders", J. Appl. Fluid Mech, **9**(4), pp. 1655-1665 (2016).

[15] Mebarek-Oudina, F., Aissa, A., Mahanthesh, B., et al. "Heat transport of magnetized Newtonian nanoliquids in an annular space between porous vertical cylinders with discrete heat source", Int Commun Heat Mass Transf, **117**, pp. 104737 (2020).

[16] Parvin, S., Nasrin, R., Alim, M. A., et al. "Thermal conductivity variation on natural convection flow of water–alumina nanofluid in an annulus", Int Commun Heat Mass Transf, **55**(19-20), 5268-5274 (2012).

[17] Selimefendigil, F., and Öztop, H. F. "Thermal and phase change process in a branching T-channel under active magnetic field and two rotating inner cylinders: Analysis and predictions by radial basis neural networks", Int. J. Heat Mass Transf, **217**, pp. 124548 (2023).

[18] Selimefendigil, F., and Öztop, H. F. "Thermal and phase change process analysis in a porous vented circular cavity under the impacts of inner rotating surface and inclined magnetic field during nanoliquid convection", J. Magn. Magn. Mate, **582**, pp. 170976 (2023).

[19] Qureshi, I. H., Nawaz, M., Abdel-Sattar, M. A., et al. ”Numerical study of heat and mass transfer in MHD flow of nanofluid in a porous medium with Soret and Dufour effects”, Heat Transf, **50**, pp. 4501-4515 (2021).

[20] Babazadeh, H., Zeeshan, A., Jacob, K., et al. ”Numerical modelling for nanoparticle thermal migration with effects of shape of particles and magnetic field inside a porous enclosure”, Iran J Sci Technol Trans Mech Eng, **45**, pp. 801-811 (2021).

[21] Khanafer, K. M., and Chamkha, A. J. ”Hydromagnetic natural convection from an inclined porous square enclosure with heat generation”, Numer Heat Transf A Appl, **33**(8), pp. 891-910 (1998).

[22] Rashad, A. M., Rashidi, M. M., Lorenzini, G., et al. ”Magnetic field and internal heat generation effects on the free convection in a rectangular cavity filled with a porous medium saturated with Cu-water nanofluid”, Int. J. Heat Mass Transf **104** pp. 878-889 (2017).

[23] EL GLILI, I., and Driouich, M. ”The Effect of Nonlinear Thermal Radiation on EMHD Casson Nanofluid over a Stretchable Riga Plate with Temperature-Dependent Viscosity and Chemical Reaction”, Phys. Chem. Res, **12**(1), pp. 157-173 (2024).

[24] Sheremet, M. A., Oztop, H. F., Pop, I., et al. ”MHD free convection in a wavy open porous tall cavity filled with nanofluids under an effect of corner heater”, Int. J. Heat Mass Transf. **103** pp. 955-964 (2016).

[25] Li, Q., Zhang, R., and Hu, P. ”Effect of thermal boundary conditions on forced convection under LTNE model with no-slip porousfluid interface condition”, Int. J. Heat Mass Transf, **167** pp. 120803 (2021).

[26] Li, Q., and Hu, P. ”Analytical solutions of fluid flow and heat transfer in a partial porous channel with stress jump and continuity interface conditions using LTNE model”, Int. J. Heat Mass Transf, **128** pp. 1280-1295 (2019).

[27] Rashidi, S., Nouri-Borujerdi, A., Valipour, M. S., et al. ”Stress-jump and continuity interface conditions for a cylinder embedded in a porous medium”, Transp Porous Media, **107**, pp. 171-186 (2015).

[28] Tahmasebi, A., Mahdavi, M., and Ghalambaz, M. ”Local thermal nonequilibrium conjugate natural convection heat transfer of nanofluids in a cavity partially filled with porous media using Buongiorno’s model”, Numer Heat Transf A App, **73** pp. 254-276 (2018).

[29] Yang, K., Chen, H., and Vafai, K. ”Investigation of the momentum transfer conditions at the porous/free fluid interface: A benchmark solution”, Numer Heat Transf A App **71** pp. 609-625 (2017).

[30] Hu, P., and Li, Q. ”Effect of heat source on forced convection in a partially-filled porous channel under LTNE condition”, Int Commun Heat Mass Transf, **114**, pp. 104578 (2020).

[31] Chamkha, A. J., and Ismael, M. A. ”Natural convection in differentially heated partially porous layered cavities filled with a nanofluid”, Numer Heat Transf A Appl, **65**(11) pp. 1089-1113 (2014).

[32] Foukhari, Y., Sammouda, M., and Driouich, M. "MHD natural convection in an annular space between two coaxial cylinders partially filled with metal base porous layer saturated by Cu–water nanofluid and subjected to a heat flux", J Therm Anal Calorim pp. 1-14 (2023).

[33] Chamkha, A. J., Groşan, T., and Pop, I. "Fully developed free convection of a micropolar fluid in a vertical channel", Int Commun Heat Mass Transf, **29**(8), pp. 1119-1127 (2002).

[34] Vijatha, M., and Reddy, P. B. A. "Entropy optimization of magnetohydrodynamic hybrid nanofluid flow with Cattaneo-Christov heat flux model. Scientia Iranica, **29**(6), pp. 3603-3618 (2022).

[35] Karimi, N., Mahmoudi, Y., and Mazaheri, K. "Temperature fields in a channel partially filled with a porous material under local thermal non-equilibrium condition an exact solution", Proc Inst Mech Eng C J Mech Eng Sci, **228**, pp. 2778-2789 (2014).

[36] Mahmoudi, Y., and Karimi, N. "Numerical investigation of heat transfer enhancement in a pipe partially filled with a porous material under local thermal non-equilibrium condition", Int. J. Heat Mass Transf, **68**, pp. 161-173 (2014).

[37] Mahmoudi, Y., and Maerefat, M. "Analytical investigation of heat transfer enhancement in a channel partially filled with a porous material under local thermal non-equilibrium condition", Int. J. Therm. Sci, **50**, pp. 2386-2401 (2011).

[38] Chamkha, A. J. "Unsteady laminar hydromagnetic fluid–particle flow and heat transfer in channels and circular pipes", Int J Heat Fluid Flow , **21**(6), pp. 740-746 (2000).

[39] Chamkha, A. J. "Non-Darcy hydromagnetic free convection from a cone and a wedge in porous media", Int. Commun. Heat Mass Transf", **23**(6), pp. 875-887 (1996).

[40] Chamkha, A. J. "Non-Darcy fully developed mixed convection in a porous medium channel with heat generation/absorption and hydromagnetic effects", Numer Heat Transf A App, **32**(6), pp. 653-675 (1997).

[41] Chamkha, A. J., Issa, C., and Khanafer, K. "Natural convection from an inclined plate embedded in a variable porosity porous medium due to solar radiation", Int. J. Therm. Sci, **41**(1), pp. 73-81 (2002).

[42] Bejan, A. "Second law analysis in heat transfer", Energy, **5**, pp. 721-732 (1980).

[43] Akhter, R., Ali, M. M., and Alim, M. A. "Entropy generation due to hydromagnetic buoyancy-driven hybrid-nanofluid flow in partially heated porous cavity containing heat conductive obstacle", Alex. Eng. J, **62**, pp. 17-45 (2023).

[44] Tayebi, T., Dogonchi, A. S., Karimi, N., et al. "Thermo-economic and entropy generation analyses of magnetic natural convective flow in a nanofluid-filled annular enclosure fitted with fins", Sustain. Energy Technol. Assess, **46**, pp. 101274 (2021).

[45] Selimefendigil, F., Chouikhi, H., and Oztop, H. F. "Natural convection and entropy generation of hybrid nanofluid in double annulus separated by a thin rotating partition under magnetic field", J. Magn. Magn. Mater, **582**, pp. 170974 (2023).

[46] Hayat, T., Nawaz, S., and Alsaedi, A. "Entropy generation analysis of peristaltic flow of magneto-nanoparticles suspended in water under second-order slip conditions", Scientia Iranica, **27**(6), pp. 3434-3446 (2020).

[47] Selimefendigil, F., Chouikhi, H., and Oztop, H. F. "Natural convection and entropy generation of hybrid nanofluid in double annulus separated by a thin rotating partition under magnetic field", J. Magn. Magn. Mater, **582**, pp. 170974 (2023).

[48] Sheikholeslami, M. "New computational approach for exergy and entropy analysis of nanofluid under the impact of Lorentz force through a porous media", Comput. Methods Appl. Mech. Eng, **344**, pp. 319-333 (2019).

[49] Sheikholeslami, M. "Numerical approach for MHD Al_2O_3-water nanofluid transportation inside a permeable medium using innovative computer method", Comput. Methods Appl. Mech. Eng, **344**, pp. 306-318 (2019).

[50] Tayebi, T., Öztop, H. F., and Chamkha, A. J. "Natural convection and entropy production in hybrid nanofluid filled-annular elliptical cavity with internal heat generation or absorption", Therm. Sci. Eng, **19**, pp. 100605 (2020).

[51] Hayat, T., Qayyum, S., Alsaedi, A., et al. "Entropy generation minimization: Darcy-Forchheimer nanofluid flow due to curved stretching sheet with partial slip", Int. Commun. Heat Mass Transf, **111**, pp. 104445 (2020).

[52] Ramasekhar, G., and Bala Anki Reddy, P. "Entropy generation on Darcy-Forchheimer flow of copper-aluminium oxide/water hybrid nanofluid over a rotating disk: Semi-analytical and numerical approaches", Scientia Iranica, **30**(6), pp. 2245-2259 (2023).

[53] Krishna, M. V., and Chamkha, A. J. "Hall and ion slip effects on Unsteady MHD Convective Rotating flow of Nanofluids—Application in Biomedical Engineering", J. Egypt. Math. Soc, **28**(1), (2020).

[54] Krishna, M. V., and Chamkha, A. J. "Hall effects on MHD squeezing flow of a water-based nanofluid between two parallel disks. Porous Media", **22**(2), (2019).

[55] Krishna, M. V., Swarnalathamma, B. V., and Chamkha, A. J. "Investigations of Soret, Joule and Hall effects on MHD rotating mixed convective flow past an infinite vertical porous plate", Journal of Ocean Engineering and Science, **4**(3), pp. 263-275 (2019).

[56] Sammouda, M., Gueraoui, K., Driouich, M., et al. "The variable porosity effect on the natural convection in a non-Darcy porous media", Int. Rev. Model. Simul, **4**, (2011).

[57] Sammouda, M., and K. Gueraoui. "MHD Double Diffusive Convection of Al2O3-Water Nanofluid in A Porous Medium Filled an Annular Space Inside Two Vertical Concentric Cylinders with Discrete Heat Flux", J. Appl. Fluid Mech, **14**, pp. 1459-1468 (2021).

[58] Singh, K. D., and Kumar, R. "Fluctuating heat and mass transfer on unsteady MHD free convection flow of radiating and reacting fluid past a vertical porous plate in slip-flow regime", J. Appl. Fluid Mech, **4**, pp. 101-106 (2011)

[59] Hussain, S., Ahmed, S. E., and Akbar, T. ”Entropy generation analysis in MHD mixed convection of hybrid nanofluid in an open cavity with a horizontal channel containing an adiabatic obstacle”, Int. J. Heat Mass Transf. **114** ,pp. 1054-1066 (2017).

[60] Sammouda, M., Gueraoui, K., Driouich, M., et al. ”Double diffusive natural convection in non-darcy porous media with non-uniform porosity”, Int. Rev. Model. Simul, **7**(6), (2013).

[61] Krane, R. J. ”Some detailed field measurements for a natural convection flow in a vertical square enclosure”, Proceedings of the First ASME-JSME Thermal Engineering Joint Conference, **1**, pp. 323-329 (1983).

[62] Abu-Nada, E., Masoud, Z., Oztop, H. F., et al. ”Effect of nanofluid variable properties on natural convection in enclosures”, Int. J. Therm. Sci, **49**(3), pp. 479-491 (2010).

[63] Sankar, M., Hong, S., Do, Y., et al. ”Numerical simulation of natural convection in a vertical annulus with a localized heat source”, Meccanica, **47**, pp. 1869-1885 (2012).

[64] Aminossadati, S. M., and Ghasemi, B. ”Natural convection cooling of a localised heat source at the bottom of a nanofluid-filled enclosure”, Eur. J. Mech. B Fluids, **28**(5), pp. 630-640 (2009).

Biographies

Foukhari Youness:

is associated with the Laboratory of Research in Physics and Engineering Sciences (LRPES), Polydisciplinary Faculty, Sultan Moulay Slimane University, as a Phd student. His research interests are on heat and mass transfer, computational fluid mechanics, nanofuids, MHD effects, porous medium, and numerical modeling.

Sammouda Mohamed:

is Professor of physics associated with the physics departmentof the Polydisciplinary Faculty, Sultan Moulay Slimane University. He is a member and founder of Laboratory of Research in Physics and Engineering Sciences (LRPES). He received his PhD from the Faculty of Sciences, Mohammed-V University. His area of research is about heat and mass transfer, computational fluid mechanics, nanofuids, MHD effects, porous medium and numerical modeling.

Driouich Mohamed:

is Professor of physics associated with the physics department of the Polydisciplinary Faculty, Sultan Moulay Slimane University. He is a member and founder of Laboratory of Research in Physics and Engineering Sciences (LRPES). He received his PhD from the Faculty of Sciences, Mohammed-V University. His area of research is about heat and mass transfer, computational fluid mechanics, nanofuids, MHD effects, porous medium and numerical modeling.

List of Tables and Figures.

Table 1: Thermophysical propreties for the hybrid nanofluid (Cu + Al_2O_3/Water).

Density	$\rho_{nf} = (1-\phi_1)\,\rho_{bf} + \phi_1.\rho_{np1}$	$\rho_{hnf} = (1-\phi_2)\,\rho_{nf} + \phi_2.\rho_{np2}$
Heat capacitance	$Cp_{nf} = (1-\phi_1)\,Cp_{bf} + \phi_1 Cp_{np1}$	$Cp_{hnf} = (1-\phi_2)\,Cp_{nf} + \phi_2 Cp_{np2}$
Thermal expansion	$\beta_{nf} = (1-\phi_1)\,\beta_{bf} + \phi_1\beta_{np1}$	$\beta_{hnf} = (1-\phi_2)\,\beta_{nf} + \phi_2\beta_{np2}$
Viscosity	$\frac{\mu_{nf}}{\mu_{bf}} = \frac{1}{(1-\phi_1)^{2.5}}$	$\frac{\mu_{hnf}}{\mu_{nf}} = \frac{1}{(1-\phi_2)^{2.5}}$
Thermal conductivity	$\frac{\lambda_{nf}}{\lambda_{bf}} = \frac{\lambda_{np1}+2\lambda_{bf}+2(\lambda_{np1}-\lambda_{bf})\phi_1}{\lambda_{np1}+2\lambda_{bf}-(\lambda_{np1}-\lambda_{bf})\phi_1}$	$\frac{\lambda_{hnf}}{\lambda_{nf}} = \frac{\lambda_{np2}+2\lambda_{nf}+2(\lambda_{np2}-\lambda_{nf})\phi_2}{\lambda_{np2}+2\lambda_{nf}-(\lambda_{np2}-\lambda_{nf})\phi_2}$
Electrical conductivity	$\frac{\sigma_{nf}}{\sigma_{bf}} = 1 + \frac{3\left(\frac{\sigma_{np1}}{\sigma_{bf}}-1\right)\phi_1}{\left(\frac{\sigma_{np1}}{\sigma_{bf}}+2\right)-\left(\frac{\sigma_{np1}}{\sigma_{bf}}-1\right)\phi_1}$	$\frac{\sigma_{hnf}}{\sigma_{nf}} = 1 + \frac{3\left(\frac{\sigma_{np2}}{\sigma_{nf}}-1\right)\phi_2}{\left(\frac{\sigma_{np2}}{\sigma_{nf}}+2\right)-\left(\frac{\sigma_{np2}}{\sigma_{nf}}-1\right)\phi_2}$

Table 2: Grid independence test.

Mesh grid	Nu_{Avg}	Error %
21×41	8.192	
31×61	8.213	0.256
41×81	8.218	0.06
51×101	8.220	0.0244
61×121	8.222	0.0243
71×141	8.224	0.0242
81×161	8.224	0

Table 3: Thermo-physical properties of water, Cu and Aluminia [64].

Properties	Units	Cu	Al_2O_3	Water
Thermal conductivity λ	$\left[W.m^{-1}.K^{-1}\right]$	401	40	0.613
Heat capacity C_p	$\left[J.Kg^{-1}.K^{-1}\right]$	385	765	4179
Density ρ	$\left[Kg.m^{-3}\right]$	8933	3970	997.1
Thermal expansion β	$\left[K^{-1}\right]$	$1.67 * 10^{-5}$	$0.85 * 10^{-5}$	$2.1 * 10^{-5}$

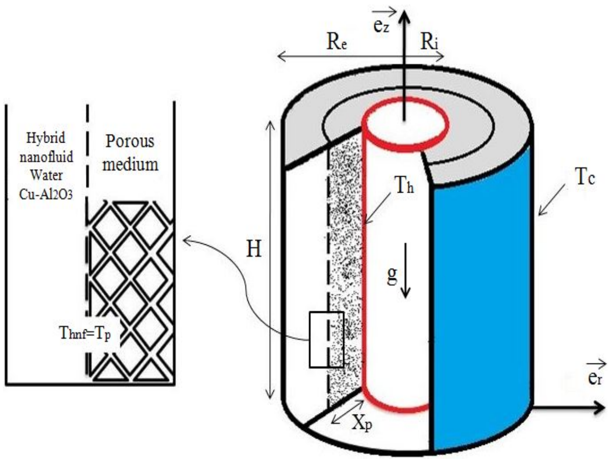

Figure 1: Schematic Physical domain.

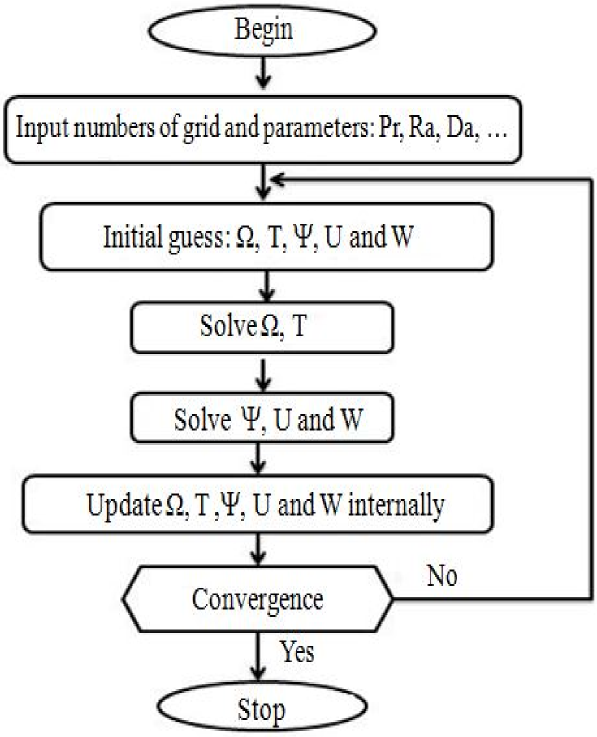

Figure 2: Flowchart for the algorithm followed.

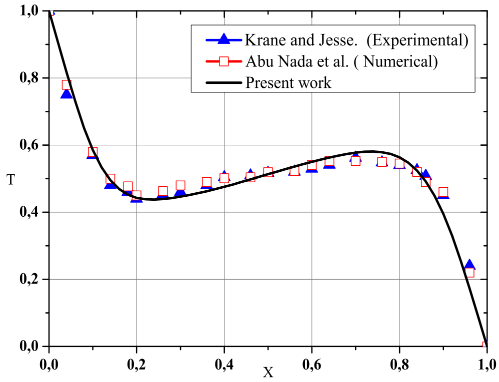

(a)

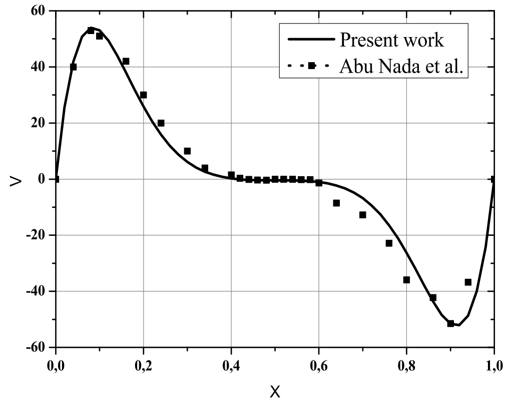

(b)

Figure 3: A comparison of our outcomes to previous research findings on temperature function (a) and velocity function (b) for Al_2O_3 ($Ra = 10^5$, Pr=0.7).

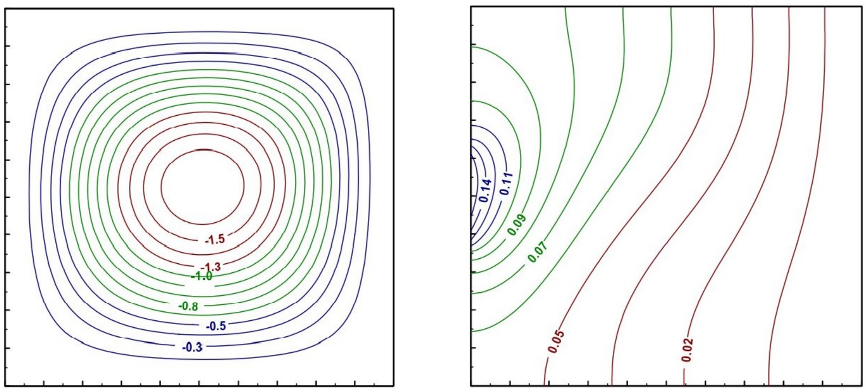

(a)

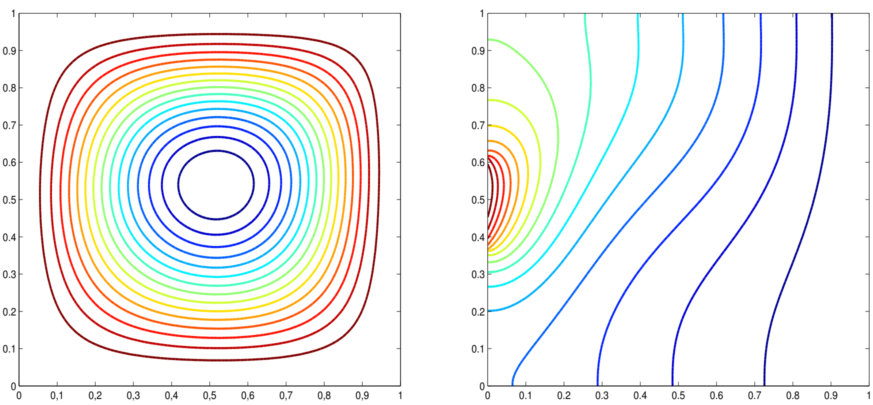

(b)

Figure 4: Streamlines and isotherms for $Ra = 10^4$ (a) Sankar et al. [59] results, (b) our results.

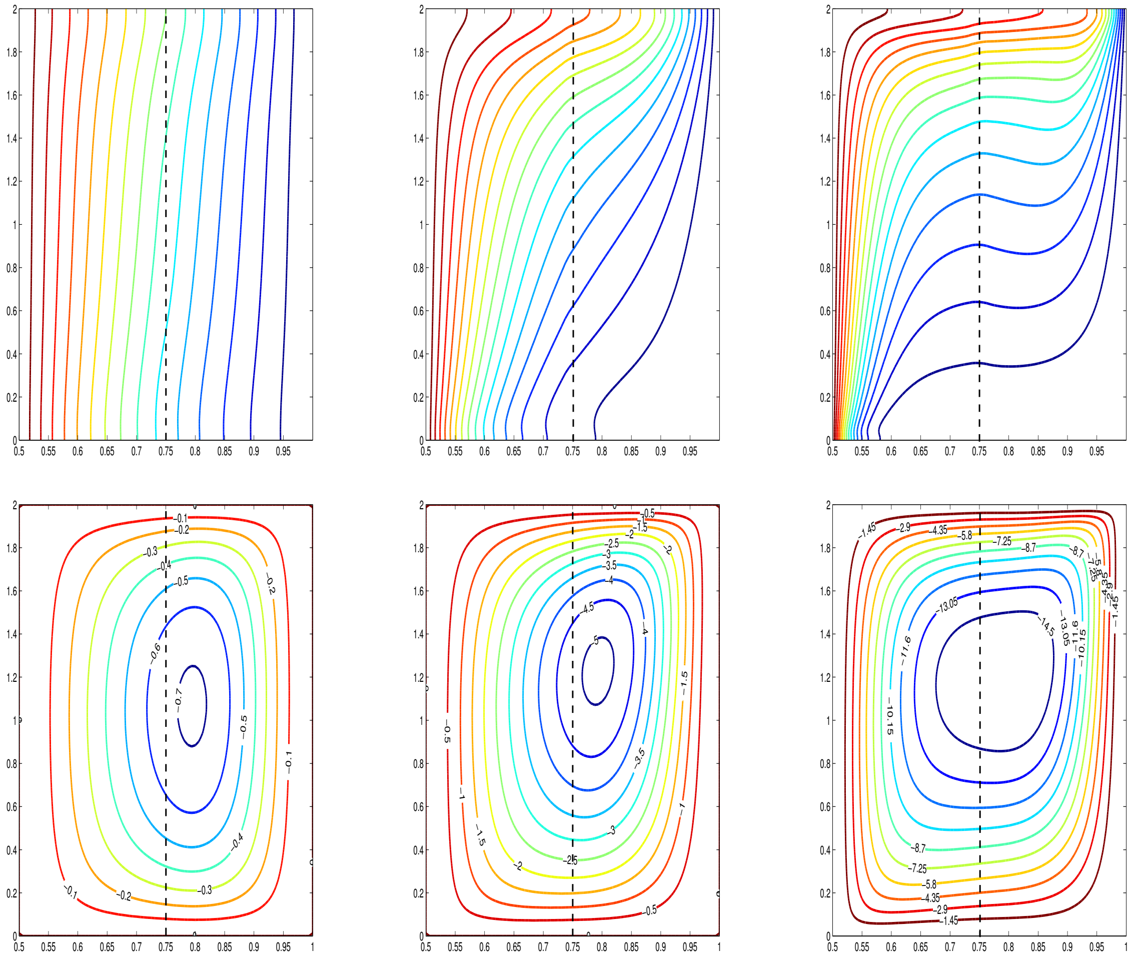

(a) (b) (c)

Figure 5: Streamlines and isotherms at Ha=50, Da=0.01 and $\phi = 4\%$ for different Rayleigh number (a)$Ra = 10^4$, (b)$Ra = 10^5$ and (c) $Ra = 10^6$.

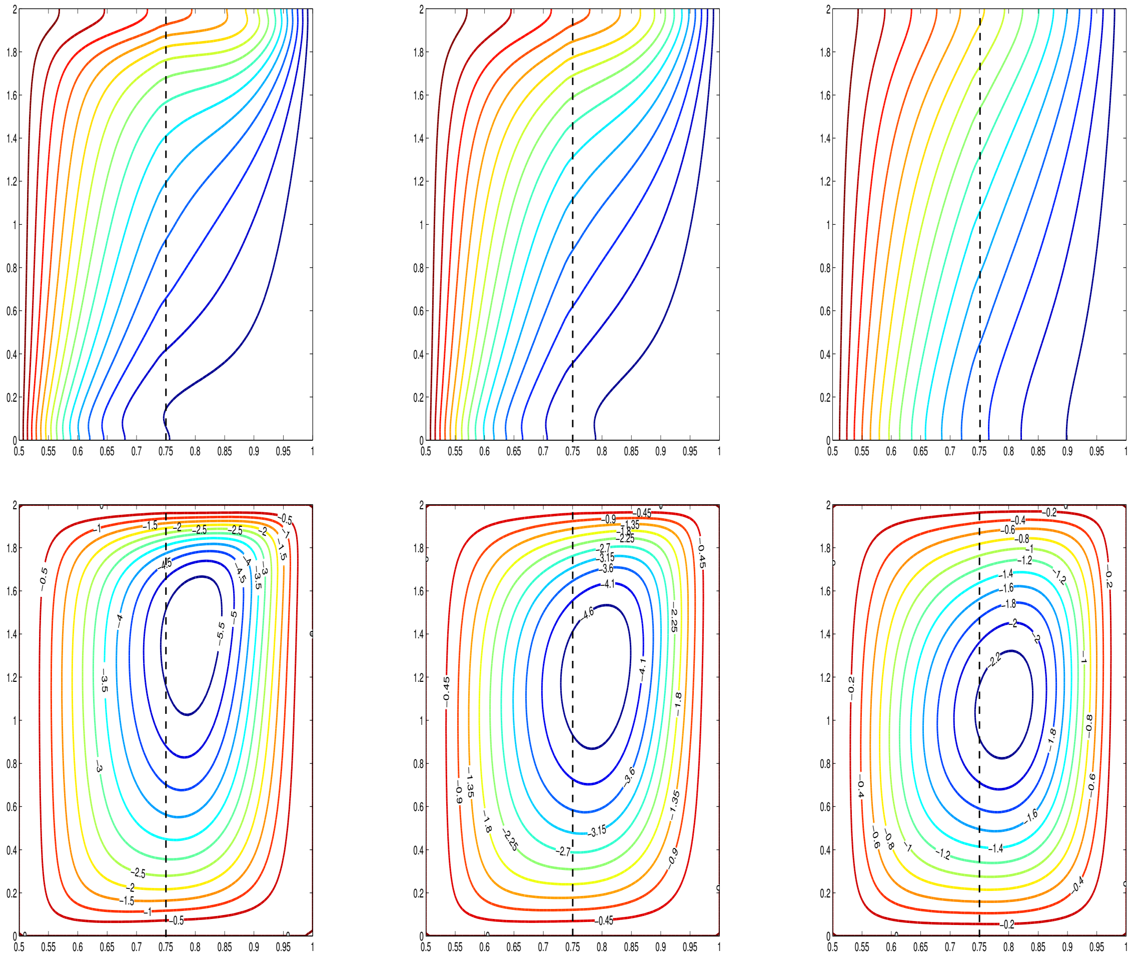

(a) (b) (c)

Figure 6: Streamlines and isotherms at $Ra = 10^5$, Da=0.01 and $\phi = 4\%$ for different Hartmann number (a)Ha=0, (b)Ha=50 and (c) Ha=150.

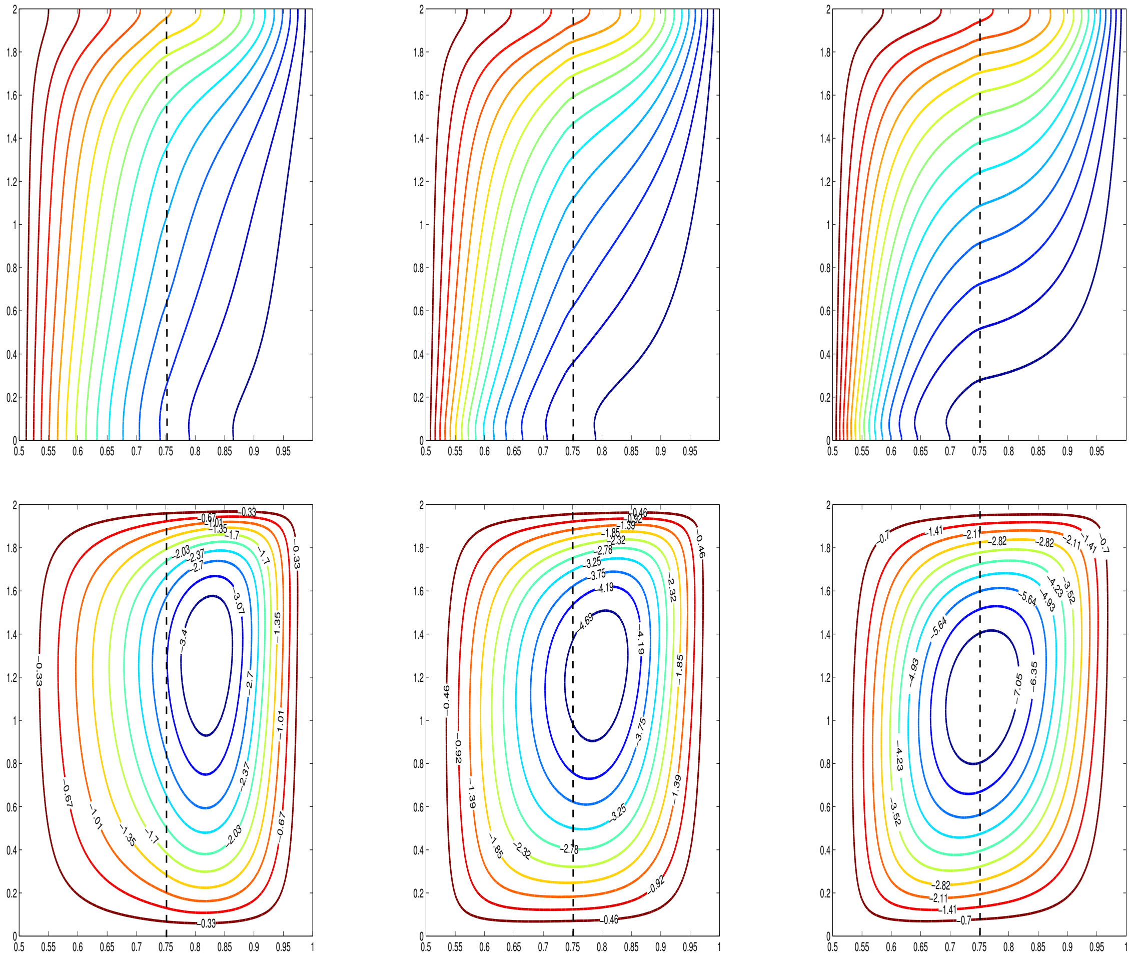

(a) (b) (c)

Figure 7: Streamlines and isotherms at $Ra = 10^5$, Ha=50 and $\phi = 4\%$ for different Darcy number (a)$Da = 10^{-5}$, (b)$Da = 10^{-3}$ and (c) $Da = 10^{-1}$.

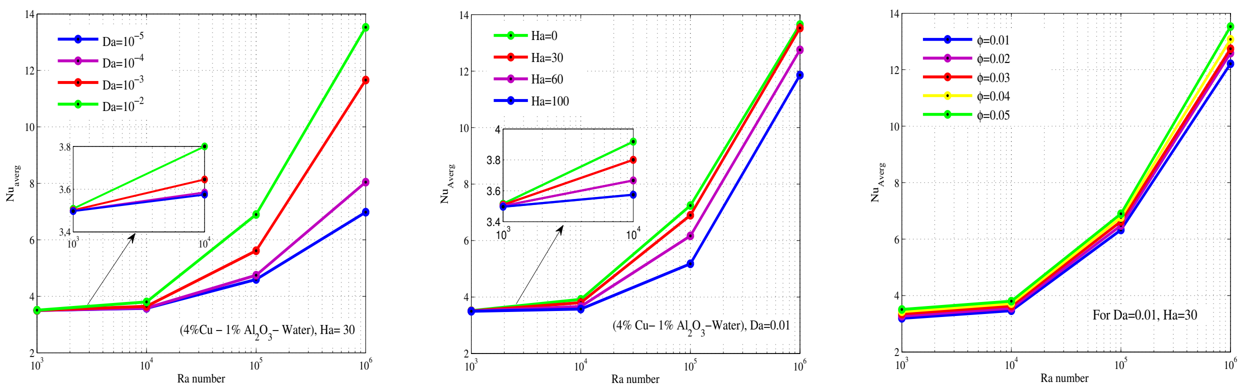

(a) (b) (c)

Figure 8: The variation of Nu_{Avg} according Ra number for different ranges (a) $10^{-5} \leq Da \leq 10^{-2}$, (b) $0 \leq Ha \leq 100$, and (c) $0.01 \leq \phi \leq 0.05$.

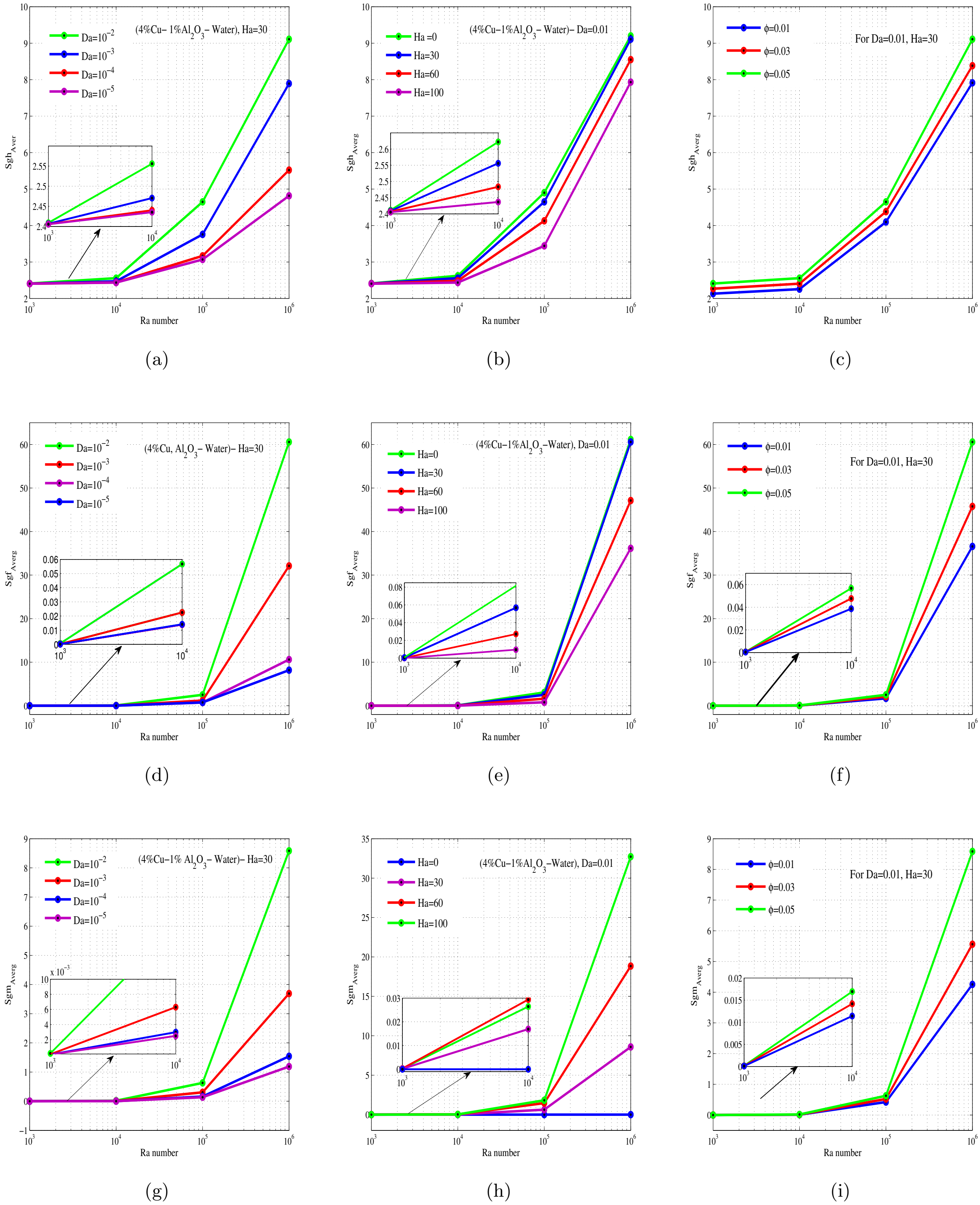

Figure 9: The variation of Nu_{Avg} component according Ra number for different ranges (a,d,g) $10^{-5} \leq Da \leq 10^{-2}$, (b,e,h) $0 \leq Ha \leq 100$, and (c,f,i) $0.01 \leq \phi \leq 0.05$.

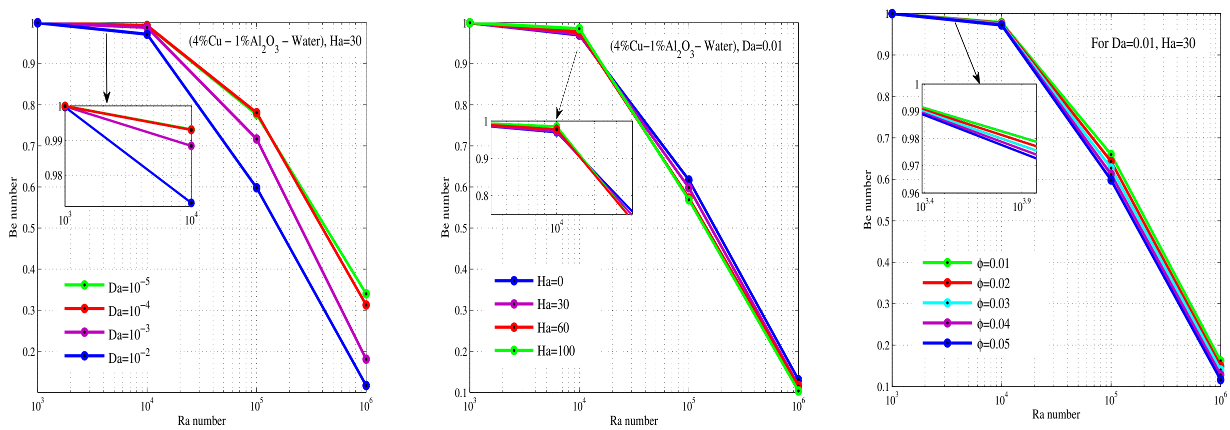

(a) (b) (c)

Figure 10: The variation of Bejan number according Ra number for different ranges (a) $10^{-5} \leq Da \leq 10^{-2}$, (b) $0 \leq Ha \leq 100$, and (c) $0.01 \leq \phi \leq 0.05$.